J. Fluid Mech. (2007), *vol.* 574, *pp.* 405–427. © 2007 Cambridge University Press
doi:10.1017/S0022112006004204 Printed in the United Kingdom

An experimental investigation on Lagrangian correlations of small-scale turbulence at low Reynolds number

MICHELE GUALA[1], ALEXANDER LIBERZON[1,2], ARKADY TSINOBER[3] AND WOLFGANG KINZELBACH[1]

[1]Institute of Environmental Engineering, Swiss Federal Institute of Technology, ETH Zurich, CH-8093 Zurich, Switzerland

[2]Department of Fluid Mechanics and Heat Transfer, Tel Aviv University, 69978 Tel Aviv, Israel

[3]Marie Curie Chair in Fundamental and Conceptual Aspects of Turbulent Flows, Institute for Mathematical Sciences and Department of Aeronautics, Imperial College, London SW7 2AZ, UK

(Received 29 August 2005 and in revised form 20 September 2006)

Lagrangian auto- and cross-correlation functions of the rate of strain s^2, enstrophy ω^2, their respective production terms $-s_{ij}s_{jk}s_{ki}$ and $\omega_i\omega_j s_{ij}$, and material derivatives, $\mathrm{D}s^2/\mathrm{D}t$ and $\mathrm{D}\omega^2/\mathrm{D}t$ are estimated using experimental results obtained through three-dimensional particle tracking velocimetry (three-dimensional-PTV) in homogeneous turbulence at $Re_\lambda = 50$. The autocorrelation functions are used to estimate the Lagrangian time scales of different quantities, while the cross-correlation functions are used to clarify some aspects of the interaction mechanisms between vorticity ω and the rate of strain tensor s_{ij}, that are responsible for the statistically stationary, in the Eulerian sense, levels of enstrophy and rate of strain in homogeneous turbulent flow. Results show that at the Reynolds number of the experiment these quantities exhibit different time scales, varying from the relatively long time scale of ω^2 to the relatively shorter time scales of s^2, $\omega_i\omega_j s_{ij}$ and $-s_{ij}s_{jk}s_{ki}$. Cross-correlation functions suggest that the dynamics of enstrophy and strain, in this flow, is driven by a set of different-time-scale processes that depend on the local magnitudes of s^2 and ω^2. In particular, there are indications that, in a statistical sense, (i) strain production anticipates enstrophy production in low-strain–low-enstrophy regions (ii) strain production and enstrophy production display high correlation in high-strain–high-enstrophy regions, (iii) vorticity dampening in high-enstrophy regions is associated with weak correlations between $-s_{ij}s_{jk}s_{ki}$ and s^2 and between $-s_{ij}s_{jk}s_{ki}$ and $\mathrm{D}s^2/\mathrm{D}t$, in addition to a marked anti-correlation between $\omega_i\omega_j s_{ij}$ and $\mathrm{D}s^2/\mathrm{D}t$. Vorticity dampening in high-enstrophy regions is thus related to the decay of s^2 and its production term, $-s_{ij}s_{jk}s_{ki}$.

1. Introduction

The evolution of velocity derivatives in a Lagrangian description, i.e. following a fluid particle, is of principal importance to the understanding of turbulent transport processes. The behaviour of fluid particles is of great interest because it describes the turbulent diffusion and transport mechanisms, which are at the core of dispersion and mixing processes (e.g. Tennekes & Lumley 1972). Since the work by Taylor (1921), Lagrangian correlations have been recognized as important statistics in the study of turbulent diffusion and dispersion (e.g. Monin & Yaglom 1971). While velocity and acceleration correlations have been exhaustively investigated both

experimentally and numerically (see Mordant, Leveque & Pinton 2004; Yeung 2002 and references therein), Lagrangian statistics of small-scale turbulence (the fields of velocity derivatives, rate of strain s^2, enstrophy ω^2 and the related processes) still represent an open field of research, owing to the lack of experimental data.

In this contribution we provide an attempt to investigate the processes of strain and enstrophy production through autocorrelation and cross-correlation functions. We start with the known aspects of strain and vorticity dynamics, as they are derived from the transport equations of the total strain, $s_{ij}s_{ij} \equiv s^2$ and enstrophy, ω^2, respectively:

$$\frac{1}{2}\frac{\mathrm{D}s^2}{\mathrm{D}t} = \underbrace{-s_{ij}s_{jk}s_{ki}}_{1}\underbrace{-\frac{1}{4}\omega_i\omega_j s_{ij}}_{2}\underbrace{-s_{ij}\frac{\partial^2 p}{\partial x_i \partial x_j}}_{3}\underbrace{+\nu s_{ij}\nabla^2 s_{ij}}_{4}, \tag{1.1}$$

$$\frac{1}{2}\frac{\mathrm{D}\omega^2}{\mathrm{D}t} = \underbrace{\omega_i\omega_j s_{ij}}_{1}\underbrace{+\nu\omega_i\nabla^2\omega_i}_{2}. \tag{1.2}$$

Both equations are valid at any time and at any point of the flow domain. They are derived from Navier–Stokes equations with no further assumptions and are extensively discussed in Tsinober (2001, Appendix C). The first term on the right-hand side of (1.1), $-s_{ij}s_{jk}s_{ki}$, is the local self-amplification process, denoted 'strain production'. This term displays a positively skewed probability density function (PDF) and, therefore, it contributes positively to $\langle \mathrm{D}s^2/\mathrm{D}t\rangle$ (Tsinober 2001), where $\langle\cdot\rangle$ denotes the average quantity. The second term in (1.1) like the first term in (1.2), $\omega_i\omega_j s_{ij}$, is associated with the vortex stretching process, it also displays a positively skewed PDF, and it plays the role of production in the enstrophy transport equation (1.2). However, enstrophy production acts not only as a production (in the mean) in (1.2), but also as a drain of 'energy' of strain as seen from the (1.1) where it appears with a minus sign. In other words the enstrophy production is also an agent of exchange of 'energy' between enstrophy and strain.

Obviously, a complete investigation of Lagrangian statistics must also include the viscous terms (i.e. term 4 in (1.1) and term 2 in (1.2)), and the pressure–strain interaction, term 3 in (1.1), which are known to be of utmost importance (e.g. Cao, Chen & Doolan 1999; Brachet *et al.* 1992; Nomura & Post 1998). Unfortunately, these terms cannot be accessed experimentally at the present stage of development of the three-dimensional-PTV measuring system.

Our first task is to study the auto- and cross-correlations of (i) the left-hand-side terms $\mathrm{D}s^2/\mathrm{D}t$ and $\mathrm{D}\omega^2/\mathrm{D}t$, (ii) the total strain and enstrophy themselves, and (iii) the production terms $-s_{ij}s_{jk}s_{ki}$ and $\omega_i\omega_j s_{ij}$. The main goal is to study the interactions between all these contributions. Our attention is thus on the pointwise relation between strain and vorticity in terms of strain and enstrophy production, with some indication of local and non-local interactions (Tsinober 2001). In fact, we can access the material derivatives $\mathrm{D}s^2/\mathrm{D}t$ and $\mathrm{D}\omega^2/\mathrm{D}t$ which also include the effects of the viscous terms (term 4 in equation (1.1) and term 2 in equation (1.2)) and of the non-local strain–pressure interaction, term 3 in equation (1.1).

In order to obtain physical insight into the mechanisms that govern the dynamics of strain and enstrophy in different flow situations and which are convected with the fluid, it is important to establish the statistics in a Lagrangian way. Fluid particles introduced into the specific flow situations of high or low strain and high or low enstrophy, would 'feel' the effect in a more persistent way and for a longer time,

compared to a point, fixed in space and in time (Tennekes & Lumley 1972). This is the motivation for us to apply Lagrangian correlation as a tool to investigate the interactions between strain, enstrophy, and their production terms, along the trajectories of fluid particles. A second motivation is to expand the experimental investigation of Lagrangian correlation by means of three-dimensional-PTV measurements, which was initiated by Lüthi, Tsinober & Kinzelbach (2005). Consistently with the previous works we will provide, along with unconditioned, conditioned statistics on strain and enstrophy magnitude. The use of conditioned statistics is also suggested by the results of Martin *et al.* (1998), Ooi *et al.* (1999), Jeong & Girimaji (2003) and Lüthi (2002), where the issue of a statistical mean cycle of evolution in the (R, Q)-plane in statistically stationary homogeneous turbulence (implying steady values for $\langle s^2 \rangle$ and $\langle \omega^2 \rangle$) was addressed. R and Q are the second and third invariants of the local velocity gradient tensor $\partial u_i/\partial x_j$, respectively. They define a phase space (R, Q-plane) where the real/complex nature of the eigenvalues of $\partial u_i/\partial x_j$ is pointwise related to both the local topology of the flow (see Chong & Perry 1990) and the small-scales processes involving strain, enstrophy and their production terms (Tsinober 2000 and Chacin & Cantwell 2000). Since R and Q are respectively equal to $-\frac{1}{3}(s_{ij}s_{ij}s_{ij} + \frac{3}{4}\omega_i\omega_j s_{ij})$ and $\frac{1}{4}(\omega^2 - 2s^2)$, it is likely that a cyclic sequence of production–destruction processes, in a statistical sense, may exist for ω^2 and s^2 also. It is quite common and natural to expect that the processes of enstrophy and strain production would depend on the level of strain and enstrophy. Therefore, for instance, in high-strain and low-enstrophy regions, there is hope of obtaining a set of portions of trajectories, which is large enough to be used to address statistically the question of how strain will decrease and how vorticity will increase. This gives further support to the decision to condition trajectory subsets, and thus correlation functions, on ω^2 and s^2.

This investigation is possible due to the recently developed three-dimensional-PTV measuring system. The intrinsic characteristics of particle tracking velocimetry made this system the most suitable tool to address issues related to the evolution of turbulent quantities along particle trajectories. This is due to two major capabilities of three-dimensional-PTV: (i) it allows measurements in a three-dimensional flow domain and estimation of the full tensor of velocity derivatives $\partial u_i/\partial x_j$, and (ii) it allows estimation of material derivatives through differentiation of any measured quantity along a particle trajectory. In the present contribution we use the data obtained by Lüthi *et al.* (2005) in homogeneous turbulence at the Taylor-microscale Reynolds number $Re_\lambda = 50$. The description of the experimental set-up and the characteristics of the three-dimensional-PTV measuring system can be found in Lüthi *et al.* (2005).

It is worth mentioning the three major limitations of the three-dimensional-PTV, and of the experimental assessment of Lagrangian correlations in general, to the best of our knowledge. The first is related to the limited capability to obtain a large sample of long trajectories in order to provide an objective estimate of the correlation functions. This is the main reason why we concentrate on the small scales of turbulence and we focus on the short-time interactions between the investigated processes. The second limitation is related to the accuracy required to resolve the velocity derivatives at the Kolmogorov scales. This imposes an additional restriction on the largest resolvable scale of the flow. Therefore it is difficult to study at the same time the small-scale interactions and the Lagrangian time scales up to the integral scales. The third limitation is of technical nature, which, at the present stage of development of three-dimensional-PTV, prevents an investigation of higher Reynolds number flows. We should point out that the results presented here need to be validated in further experiments and possibly by numerical simulations.

The paper is organized as follows. In § 2 the issues concerning the estimation of correlation functions from finite samples are presented and three different estimators are introduced. Section 3 is dedicated to the experimental results. First, the autocorrelation functions are shown and the Lagrangian integral time scales of the various quantities of interest are estimated. Second, the trajectory subsets conditioned on strain and enstrophy magnitudes are introduced and their effect on the autocorrelation functions is discussed. Third, the full set of unconditioned and conditioned cross-correlation functions is presented and interpreted, with particular emphasis on the comparison between the three different estimators. A discussion and conclusions follow.

2. Numerical procedure

Obtaining Lagrangian correlation from experimental data available through three-dimensional-PTV has some intrinsic difficulties due to the limited spatial extent of our measuring volume (side length of the order of 10 Kolmogorov length scales), and due to the dependence of the spatial resolution on the mean inter-particle distance. Higher spatial resolution requires an increasing number of tracing particles. The linking efficiency depends mainly on the ratio between the mean particle displacement between two consecutive frames and the mean inter-particle distance within the same frame (see Lüthi *et al.* 2005). Therefore, for high velocity or high acceleration, where the particle displacement increases significantly, we have to cope with a decrease in the linking efficiency and an increased probability of losing particles, thus limiting the lengths of the obtained trajectories. The main drawback, though not new (see for example, Mordant *et al.* 2004) is that the recorded long trajectories are likely to belong to a biased subset of weak turbulence. We will show below that different parameters and estimators of correlation functions can be used to quantify the bias associated with the varying length of the trajectories. The first estimator is a biased estimator (Priestley 1981) defined

$$\rho_{XY}(\tau) = \frac{\dfrac{1}{N}\displaystyle\sum_{N} R_{XY}(\tau)}{[Var(X)Var(Y)]^{1/2}} \tag{2.1}$$

where R_{XY} denotes the covariance of the two Lagrangian quantities X and Y along a single trajectory formed by N_{ti} linked points:

$$R_{XY}(\tau) = \langle (X(t+\tau) - \mu_X)(Y(t) - \mu_Y) \rangle_{N_{ti}}. \tag{2.2}$$

Note that the sum in equation (2.1) is operating along the whole set of N trajectories, and the variance $Var(X)$ and the mean μ_X, are defined as:

$$\mu_X = \frac{1}{N_p}\sum_{N_p} X, \quad Var(X) = \frac{1}{N_p}\sum_{N_p}(X - \mu_X)^2 \tag{2.3}$$

where N_p is the total number of points obtained by counting all the points of all individual trajectories, i.e. $N_p = \sum_N N_{ti}$

The estimator given in equation (2.1), is significantly influenced, as we show here, by two parameters: the number of linked points (in time) forming each trajectory N_{ti} (which varies for different trajectories), and the maximum time lag, denoted here as M.

Each particle is tracked for a time interval of $L_{ti} = N_{ti}\Delta t$ (where $\Delta t = 1/60$ s is the temporal resolution of the cameras). In the following we refer to the time interval

L_{ti} as the trajectory length. It is normalized with the Kolmogorov time scale τ_η. The maximum time lag M is the necessary parameter that we introduce in order to be able to sum the contributions of all trajectories. For the estimation of the Lagrangian integral time scales, M has to be longer than the time scale of the investigated quantities, implying that short trajectories cannot be used for this purpose. On the other hand, a set of long trajectories may not be large enough for the correlations to converge and, as we have mentioned, may also bias the results towards the behaviour of weakly turbulent regions. We shall demonstrate how a properly chosen maximum lag M and a sufficiently large subset of long trajectories (i.e. longer than M) reduce the aforementioned bias.

We compute the Lagrangian correlation functions by using different subsets of trajectories, each subset having a different minimum trajectory length threshold, ranging from $4\tau_\eta$ to $14\tau_\eta$. In order to sum all the contributions to the correlation function $\rho_{XY}(\tau)$, the time lag τ was chosen to span a fixed range $[-M : M]$ for all trajectories. First, we show in figure 1(a–c) mean and variance values of some of the investigated quantities for the different thresholds. In this figure we depict the mean values $\mu_{\hat{X}}$ and variances $Var(\hat{X})$ of the respective quantities, calculated on a subset of trajectories longer than the prescribed threshold, e.g. $\hat{X}(\tau/\tau_\eta = 4) = X(L_{ti}/\tau_\eta > 4)$, and normalized with the mean (μ_X) and variance ($Var(X)$) of the whole dataset. As we mentioned above, the bias of long trajectories towards weaker values is the main drawback of Lagrangian measurements and can be seen in figure 1(a–c). Second, we show in figure 1(d–g) auto- and cross-correlation functions calculated with the first estimator ρ_{XY}. Each curve represents the correlation function computed on a trajectory subset which comprises trajectories longer than a certain threshold, as defined above as a function of τ_η. Though the dependence on the trajectory length is visible, mostly for the tails in the autocorrelation curves of the long-scale processes (e.g. velocity), the qualitative behaviour of the depicted functions is not significantly affected. For the short-scale processes (figure 1f, g), the bias is substantially weaker. We acknowledge here that the correlation functions of the long-scale processes could be underestimated.

An intrinsic difficulty in the Lagrangian analysis is that the time series of any quantity of interest, along each single trajectory of finite length, are not likely to display zero average, thus causing a bias in the correlations calculated through estimator ρ_{XY}. In order to overcome this problem, we propose a second estimator $\overline{\rho_{XY}}(\tau)$ defined as

$$\overline{\rho_{XY}}(\tau) = \frac{1}{N}\sum_{N}\left[\frac{\langle (X(t+\tau)-\mu(X)_{ti})(Y(t)-\mu(Y)_{ti})\rangle}{[Var(X)_{ti}\,Var(Y)_{ti}]^{1/2}}\right] \tag{2.4}$$

where

$$\mu(X)_{ti} = \frac{1}{N_{ti}}\sum_{N_{ti}} X, \quad Var(X)_{ti} = \frac{1}{N_{ti}}\sum_{N_{ti}}(X-\mu(X)_{ti})^2. \tag{2.5}$$

This estimator is the average of N correlation functions, each calculated along a trajectory and normalized using the average $\mu(X)_{ti}$ and variance $Var(X)_{ti}$ of the trajectory. We should stress that, though $\mu(X)_{ti}$, calculated on single trajectories, can vary significantly, the average over the whole N trajectories is equal to μ_X computed on the whole dataset. Averaging different correlation functions implies that each trajectory gives the same contribution to the averaged $\overline{\rho_{XY}}(\tau)$ regardless of its variance. Therefore, strong events which are reflected in some trajectories and significantly affect $R_{XY}(\tau)$ contribute with a different weight (i.e. variance) to the

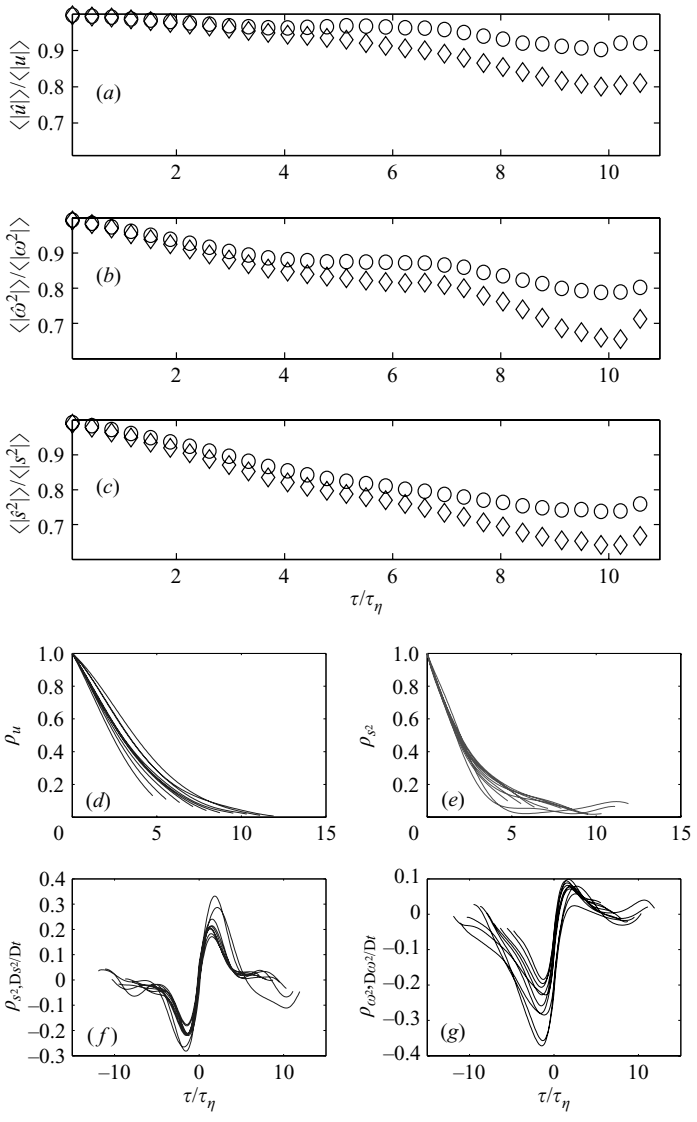

FIGURE 1. Mean $\mu_{\hat{X}}$ ($\circ$) and variance $Var(\hat{X})$ ($\diamond$) values of (a) the velocity magnitude, (b) enstrophy, and (c) strain, calculated for different thresholds of the minimum trajectory length, and normalized with the corresponding value for the whole dataset. Lagrangian correlation functions for different thresholds of the minimum trajectory length ((d) autocorrelation of one velocity component, (e) strain, (f) cross-correlations $\rho_{s^2,\mathrm{D}s^2/\mathrm{D}t}$, ($g$) $\rho_{\omega^2,\mathrm{D}\omega^2/\mathrm{D}t}$).

aforementioned estimators $\rho_{XY}(\tau)$ and $\widehat{\rho_{XY}}(\tau)$. In order to single out the effect of the different weighting, we propose a third estimator which combines the principles of the first two, using the averages of single trajectories but without normalizing the covariances for each trajectory:

$$\widehat{\rho_{XY}}(\tau) = \frac{\sum_N \langle (X(t+\tau) - \mu(X)_{ti}) \cdot (Y(t) - \mu(Y)_{ti}) \rangle}{\sum_N [Var(X)_{ti}\, Var(Y)_{ti}]^{1/2}} \tag{2.6}$$

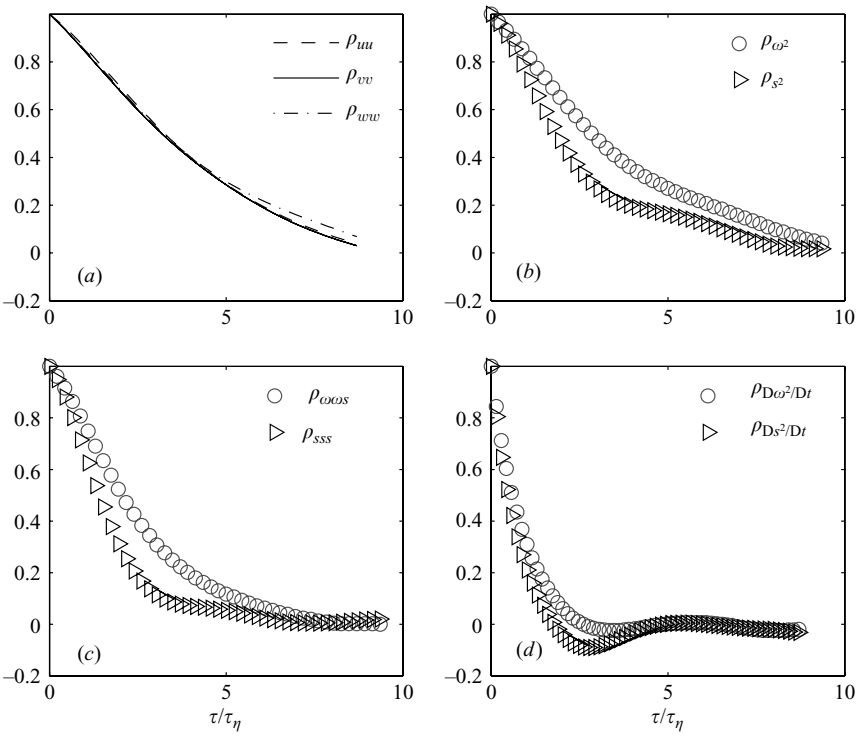

FIGURE 2. Lagrangian autocorrelation functions of (*a*) the three velocity components, (*b*) strain and enstrophy, (*c*) strain and enstrophy production terms and (*d*) strain and enstrophy material derivatives.

As we will show, equations (2.4) and (2.6) lead to similar results if we exclude from the whole dataset the trajectories which display high variances $Var(X)_{ti}$.

The next section is devoted to the presentation of the results. We first show autocorrelation functions $\rho_{XX}(\tau)$ and derive the Lagrangian time scales of the different quantities of interest. This is done in order to discuss the differences between the results of the three estimators in the case of cross-correlation functions. Note that the second and the third estimators are used in the specific context of estimating cross-correlation from the experimental dataset of trajectories of finite length. The main point is to provide a tool to clarify the behaviour of small-scale processes under the effect of strong events (with large variance).

3. Results

3.1. *Lagrangian autocorrelation functions*

We show in figure 2 the one-side autocorrelation functions, $\rho_{XX}(\tau)$, estimated using equation (2.1). We note from figure 2(*b*) that enstrophy and strain exhibit longer Lagrangian correlation time scales than the respective production terms (figure 2*c*). In addition, ω^2 exhibits a longer time scale than s^2, which is in agreement with the results of Yeung & Pope (1989) and Pope (1990) and with the experimental observation of Andreotti, Douady & Couder (2001) in which the intrinsic instability of pure strain regions is pointed out. Also, the strain production $-s_{ij}s_{jk}s_{ki}$ manifests a shorter correlation with respect to the enstrophy production $\omega_i\omega_j s_{ij}$ (figure 2*c*). In

T_u	T_v	T_w	T_{ω^2}	T_{s^2}	$T_{\omega\omega s}$	T_{sss}	$T_{\mathrm{D}\omega^2/\mathrm{D}t}$	$T_{\mathrm{D}s^2/\mathrm{D}t}$
3.7	3.6	3.7	3.6	2.6	2.5	1.7	0.7	0.4

TABLE 1. Lagrangian integral time scales of the quantities of interest, normalized with the Kolmogorov time scale, τ_η as estimated from the autocorrelation functions in figure 2.

table 1 we report the Lagrangian integral time scales T_X of the quantities of interest, computed as an integral of the correlation function $\rho_{XX}(\tau)$, normalized with the Kolmogorov time scale, τ_η. We acknowledge that we underestimate the Lagrangian integral time scale of enstrophy compared to the results of Yeung (2001) ($T_{\omega^2} = 5.32$ at $Re_\lambda = 38$) and Yeung & Pope (1989) ($T_{\omega^2} = 5.66$ at $Re_\lambda = 54$). This is due to the limited length of our trajectories compared to the time scale of enstrophy, combined with the effect of the biased estimator. For the same reason, we also underestimate the Lagrangian integral time scale of the velocity components. However, our estimate of T_{s^2} is much closer to the one provided by these authors (2.81 at $Re_\lambda = 38$ and 2.95 at $Re_\lambda = 54$). This means that we are also able to capture the shorter-scale processes that we are mostly interested in, such as strain and enstrophy production (figure 2*c*).

Comparing figures 2(*c*) and 2(*d*), we observe that enstrophy production $\omega_i\omega_j s_{ij}$ is a slower process compared to the material derivative of enstrophy, $\mathrm{D}\omega^2/\mathrm{D}t$. From this we infer that the effect of the viscous term is not negligible for the short-term interaction of the order of the Kolmogorov time scale, τ_η (see also Lüthi *et al.* 2005). Similar conclusions can be drawn by comparing the autocorrelation curves of the strain production term at short time lags with the curve of the material derivative $\mathrm{D}s^2/\mathrm{D}t$. It is noteworthy that in the ideal case of stationary homogeneous turbulence in unbounded space the autocorrelations of $\mathrm{D}\omega^2/\mathrm{D}t$ and $\mathrm{D}s^2/\mathrm{D}t$ should provide zero integral time scale (see e.g. Monin & Yaglom 1971). However the statistical homogeneity and stationarity of the flow (in the Eulerian sense) is not reflected equivalently by a limited subset of long trajectories. Consequently the Lagrangian integral time scales of $\mathrm{D}\omega^2/\mathrm{D}t$ and $\mathrm{D}s^2/\mathrm{D}t$ are expected to be small at best.

Despite the limitations in the estimate of the Lagrangian integral time scales discussed above, we stress that the qualitative behaviour of the autocorrelation functions of the quantities of interest are in agreement with the numerical and experimental results in the literature. For example, the enstrophy autocorrelation function is very similar to that of the velocity component (though both underestimated), in agreement with the results of Yeung (2001), at similar Re_λ. Therefore we emphasize only the comparative analysis of the autocorrelation curves presented which indicates that different processes contribute to the transport equations of strain and enstrophy (1.1) and (1.2) with different time scales.

3.2. *Conditioned autocorrelation functions*

The main purpose of the conditioned autocorrelation function analysis is to study the scales of the processes in the regions of qualitatively different levels of strain and enstrophy. On the one hand the portion of trajectories along which s^2 and ω^2 can satisfy certain conditions based on their respective magnitudes (e.g. high-strain, high-enstrophy) are expected to be shorter than the integral time scales of strain and enstrophy. On the other hand the minimal length of the portion of the trajectory used for this analysis cannot be much shorter than the time scales of the processes under investigation (e.g. strain production). As we learn from the results shown above (figure 2 and table 1), at this low Reynolds number flow, the autocorrelation functions

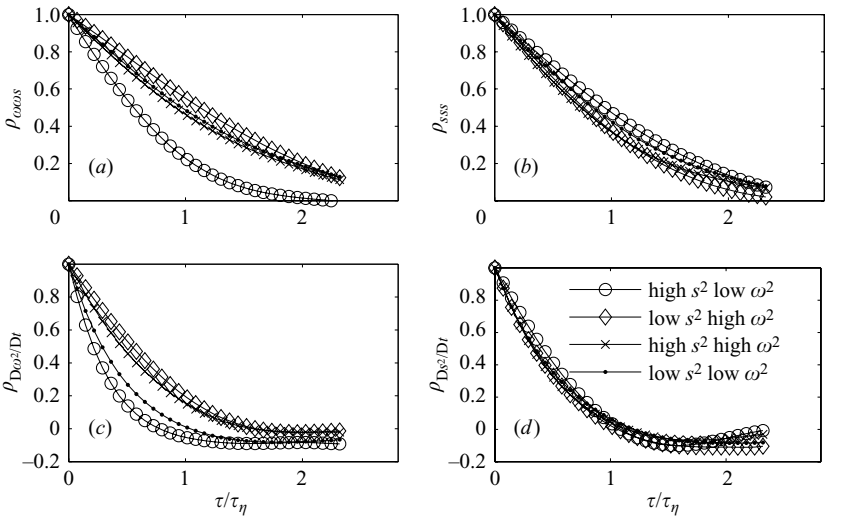

FIGURE 3. Lagrangian autocorrelation of (*a*) $\omega_i\omega_j s_{ij}$, (*b*) $s_{ij}s_{jk}s_{ki}$, (*c*) $\mathrm{D}\omega^2/\mathrm{D}t$ and (*d*) $\mathrm{D}s^2/\mathrm{D}t$, conditioned on the strain and enstrophy distribution.

of strain and enstrophy production terms and of their material derivatives display small values within $3\tau_\eta$ (e.g. ρ_{sss} is approximately 0.2 at $\tau = 2.5\tau_\eta$, in figure 2*c*). This implies that $2.5\tau_\eta$ could be used as a reasonable compromise for the minimal length of the trajectory used for the following conditional analysis.

The conditioned autocorrelation functions of $-s_{ij}s_{jk}s_{ki}$, $\omega_i\omega_j s_{ij}$, $\mathrm{D}s^2/\mathrm{D}t$ and $\mathrm{D}\omega^2/\mathrm{D}t$ are computed for the four cases: (i) high-strain–low-enstrophy, (ii) high-strain–high-enstrophy, (iii) low-strain–high-enstrophy, (iv) low-strain–low-enstrophy. We also define the threshold values that correspond to 'high' and 'low' values for enstrophy and strain in two ways: (*a*) taking into account the distributions of s^2 and ω^2, 'high' and 'low' are defined such as to include the top and bottom 30 % of their distributions respectively (figure 3); (*b*) 'high' and 'low' are defined as larger and smaller than the mean values μ_{ω^2} and μ_{s^2}, respectively (figure 4). While the latter is more commonly used, the former takes into account the fact that the distributions of s^2 and ω^2 are not Gaussian. Therefore we believe that both conditions are representative and useful in this context. As we show below, in our flow the two sets of conditioned correlation functions show similar trends, though in the first case the differences between the four conditions are more evident. It is also clear that the more strict the condition is, the fewer satisfactory trajectory portions can be found and the less representative are the related statistics.

We show in figures 3(*a*, *b*) and 4(*a*, *b*) the one-sided autocorrelations of the enstrophy and strain production terms, computed with the four different conditions defined above. We note that in high-strain–low-enstrophy regions, enstrophy production exhibits the shortest autocorrelation and we infer that this is possibly due to shear instabilities which are apparently higher in these regions as pointed out by Vincent & Meneguzzi (1994) and Andreotti *et al.* (2001). Moreover, $\omega_i\omega_j s_{ij}$ manifests the slowest decay in the case of high-enstrophy–low-strain. This can be related to the idea of Constantin (1994) who inferred that in high-enstrophy regions viscosity contributes to the formation of spatially coherent vorticity resulting in a slow dampening of intense vortex filaments (see also the longer scale of $\mathrm{D}\omega^2/\mathrm{D}t$ in figure 3*c*). In the case of strain production $-s_{ij}s_{jk}s_{ki}$, the differences are less marked which is consistent with

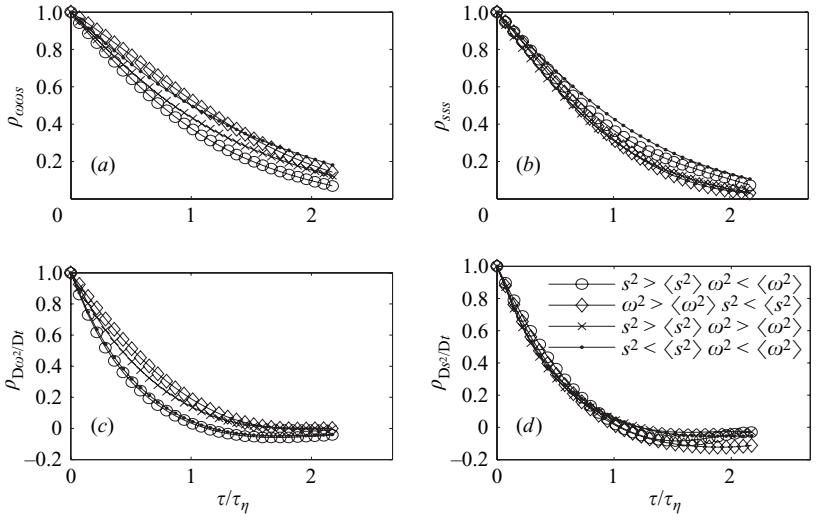

FIGURE 4. Lagrangian autocorrelation of (*a*) $\omega_i\omega_j s_{ij}$, (*b*) $s_{ij}s_{jk}s_{ki}$, (*c*) $\mathrm{D}\omega^2/\mathrm{D}t$ and (*d*) $\mathrm{D}s^2/\mathrm{D}t$, conditioned on strain and enstrophy magnitude.

the fact that strain production is a self-amplification process (Tsinober 2001). The shortest correlation is found for low-strain–high-enstrophy. We can infer that this is due to the effect of both the low-strain condition and the preferential high rotation of the eigenframe of the rate of strain tensor in high-enstrophy regions (Guala *et al.* (2005)). This might also explain why $-s_{ij}s_{jk}s_{ki}$ manifests a similar behaviour in the conditions of high-strain–low-enstrophy and low-strain–low-enstrophy.

In figures 3(*c*, *d*) and 4(*c*, *d*) the one-sided autocorrelation of the material derivatives of enstrophy and strain are shown. By comparing figures 3(*a*) and 3(*c*) (or figures 4(*a*) and 4(*c*), we note that $\mathrm{D}\omega^2/\mathrm{D}t$ becomes less correlated in low-enstrophy–high-strain regions, where the production term $\omega_i\omega_j s_{ij}$ also manifests the shortest correlation. The same is true in the case of high-enstrophy–low-strain, where both $\mathrm{D}\omega^2/\mathrm{D}t$ and $\omega_i\omega_j s_{ij}$ show the slowest decay.

The fact that $\mathrm{D}s^2/\mathrm{D}t$ and $\mathrm{D}\omega^2/\mathrm{D}t$ autocorrelations decay faster than the respective contributing production terms (shown in figure 3*a*, *b*) suggests that the strain–pressure and the viscous terms (terms 3 and 4 in equation (1.1), term 3 in equation (1.2)) have a significant effect on the dynamics of the total strain and enstrophy.

3.3. *Cross-correlation functions*

We proceed to the estimation of unconditioned Lagrangian cross-correlation functions shown in figure 5. The main focus of the present section is to single out some aspects of the interaction between strain and enstrophy, regardless of their magnitude, and to discuss the effects of the different estimators on the correlation functions.

We observe different shapes of the cross-correlation curves of different quantities: in the case of ρ_{ω^2,s^2} the highest correlation value is at $\tau = 0$ (figure 5*a*); $\rho_{s^2,\mathrm{D}s^2/\mathrm{D}t}$ and other curves in figure 5(*b*, *c*) show weak correlation at $\tau = 0$ and the peak is shifted by a certain time lag. Here we interpret the latter shape as evidence of a 'cause-consequence' relationship between the first quantity in our notation (e.g. s^2 in $\rho_{s^2,\mathrm{D}s^2/\mathrm{D}t}$) and the second quantity. This means that, for example, s^2 'follows' $\mathrm{D}s^2/\mathrm{D}t$ or, in other words, high and positive $\mathrm{D}s^2/\mathrm{D}t$ induces high s^2 after roughly $2\tau_\eta$. This is also true in the opposite direction, for instance negative slope of s^2 ($\mathrm{D}s^2/\mathrm{D}t < 0$)

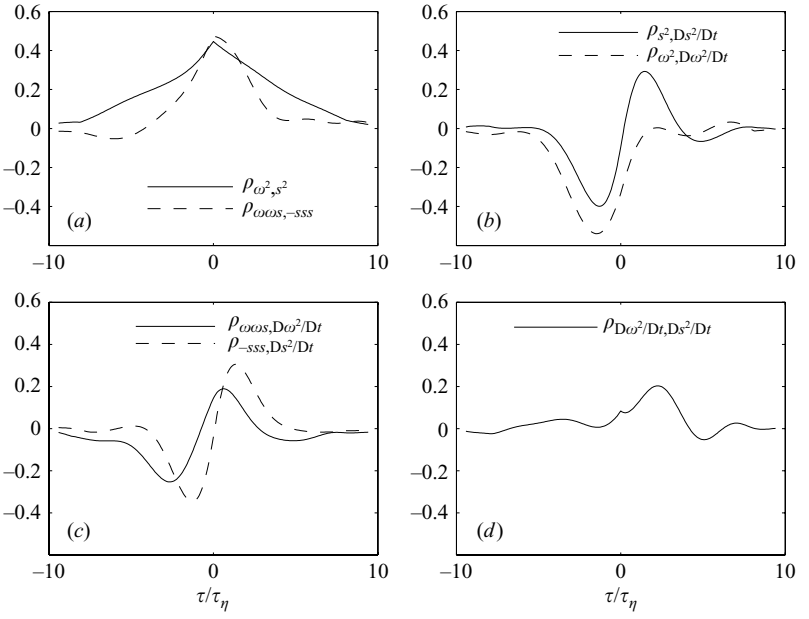

FIGURE 5. Lagrangian cross-correlation functions between different processes involving strain and enstrophy (computed through the estimator ρ_{XY}, equation (2.2)).

at $\tau = -2\tau_\eta$ statistically leads to $s^2 < \mu_{s^2}$; if this is not the case (e.g. for $\rho_{\mathrm{D}\omega^2/\mathrm{D}t,\mathrm{D}s^2/\mathrm{D}t}$) it means that the 'cause–consequence' relationship is statistically relevant only in one direction, e.g. $\mathrm{D}s^2/\mathrm{D}t$ induces $\mathrm{D}\omega^2/\mathrm{D}t$. Here we can discuss causal relationships because the quantities under investigation are related by equations (1.1) and (1.2), and also because strain and enstrophy are parts of the same velocity gradient tensor. A more subtle interpretation of the cross-correlation functions concerns the case in which the highest correlation value is at $\tau = 0$, and the curve is skewed to one of the sides. For example, the skewness and the shift of the peak of ρ_{ω^2,s^2} towards positive time lag, as reported by Yeung & Pope (1989) and Mordant *et al.* (2004), suggests that ω^2 tends to increase with time after the action of strain, due to the statistical prevalence of vortex stretching over vortex compression.

In our results (figure 5*a*) we note that ω^2 and s^2 manifest positive correlation coefficients ($\rho_{\omega^2,s^2}(\tau = 0) \approx 0.5$), which is in agreement with the numerical results of Yeung & Pope (1989) and Mordant *et al.* (2004). However, we do not observe skewness or the shift of the peak of this cross-correlation function. The same level of correlation, at zero time lag, is observed in figure 5(*a*) between $\omega_i\omega_j s_{ij}$ and $-s_{ij}s_{jk}s_{ki}$, while $\mathrm{D}\omega^2/\mathrm{D}t$ and $\mathrm{D}s^2/\mathrm{D}t$ are correlated only after a certain time lag (figure 5*d*). In addition, from the cross-correlation functions between $\omega_i\omega_j s_{ij}$ and $\mathrm{D}\omega^2/\mathrm{D}t$ and between $-s_{ij}s_{jk}s_{ki}$ and $\mathrm{D}s^2/\mathrm{D}t$, we can infer that the shifted peak of the cross-correlation after a certain time lag is more evidence of the non-local effects on the material derivatives caused by the additional terms in equations (1.1) and (1.2). This shift is even more pronounced in the case of $\rho_{-sss,\mathrm{D}s^2/\mathrm{D}t}$ possibly due to the effect of the strain–pressure term in equation (1.1).

Before proceeding further with the physical interpretation of our results, we should to stress the effects that different correlation estimators have on the cross-correlation functions. The cross-correlation functions presented in figure 5 are computed using the estimators $\overline{\rho_{XY}}(\tau)$, equation (2.4), and $\widehat{\rho_{XY}}(\tau)$, equation (2.6), and shown in figures 6

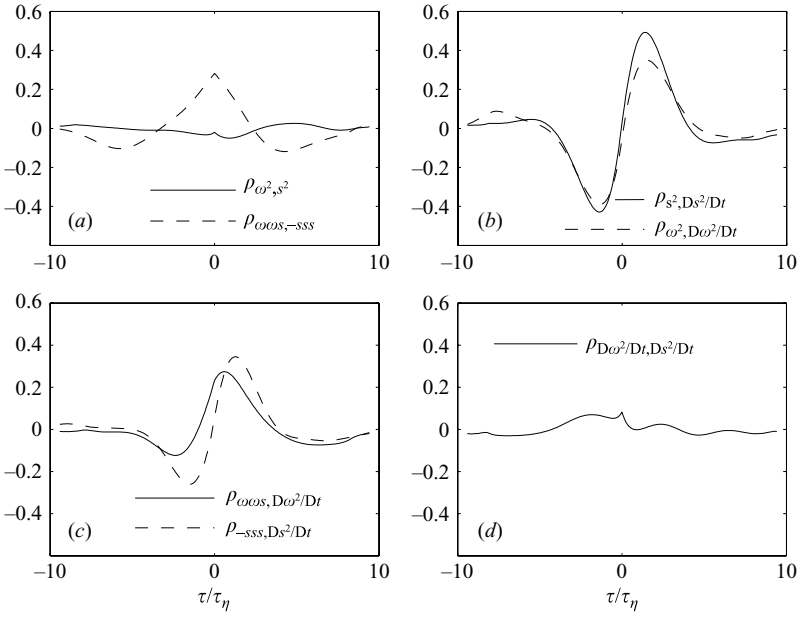

FIGURE 6. Lagrangian cross-correlation functions between different processes involving strain and enstrophy, computed through $\overline{\rho_{XY}}$, averaging single trajectory correlation functions, as described in equation (2.4)).

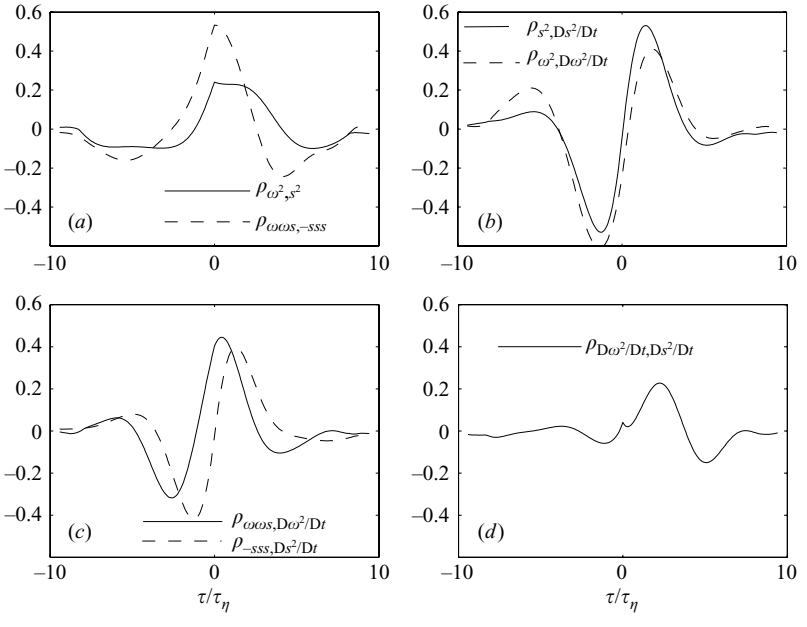

FIGURE 7. Lagrangian cross-correlation functions between different processes involving strain and enstrophy, computed through $\widehat{\rho}_{XY}$ biased correlation subtracting each trajectory's mean, equation (2.6)).

and 7, respectively. As we have shown in § 3.1, ω^2 and s^2 exhibit long autocorrelation curves, with tails that approach zero correlation values at roughly $10\tau_\eta$ (corresponding to roughly 2 to 3 times their integral time scales; see table 1). By using the first

estimator we have a situation in which s^2 and ω^2 along some of the trajectories are more than twice their means μ_{s^2} and μ_{ω^2}, respectively. In this case ρ_{XY} will be significantly biased towards positive values, regardless of the mutual evolution of $s^2(\tau)$ and $\omega^2(\tau)$ along the particle trajectory. In other words, assuming for example that both s^2 and ω^2 behave along a trajectory as perfect sines with high mean values $\mu_{s^2_{ti}}$, $\mu_{\omega^2_{ti}}$ and with a certain phase delay between them, their cross-correlation curve will look like any autocorrelation curve, with no information about the phase shift, i.e. their mutual evolution. An analogous situation occurs for $\omega_i\omega_j s_{ij}$ and $-s_{ij}s_{jk}s_{ki}$, which also present positive mean values and positively skewed PDFs. Their cross-correlation $\rho_{\omega\omega s,-sss}$ is again biased towards positive values.

We should also note that each trajectory contributes to $\langle (X(t)-\mu_X)(Y(t+\tau)-\mu_Y)\rangle$ with a different weight, depending on how much $\mu_{X_{ti}}$ differs from μ_X. Therefore, strong turbulent events (say, high s^2–high ω^2), though rare, may contribute significantly to $\langle (X(t)-\mu_X)(Y(t+\tau)-\mu_Y)\rangle$ and enhance the bias mentioned above. This is, however, expected to be more pronounced for the quantities that have an integral time scale comparable to the minimal trajectory length used in the correlation analysis, such as ω^2 and s^2, rather than their production terms or their derivatives, which exhibit shorter integral time scales. In other words, the probability of finding a long portion of trajectory where $s^2(\tau) > \mu_{s^2}$ is higher than the probability of finding a long portion where $-s_{ij}s_{jk}s_{ki}(\tau) > \langle \mu_{-sss}\rangle$.

Using the second estimator $\overline{\rho_{XY}}$ (equation (2.4)), strain and enstrophy exhibit a vanishing correlation, shown as solid line in figure 6*a*). $\overline{\rho_{\omega\omega s,-sss}}$, though affected, maintains some correlation, while the other (shorter-scale) processes, involving the material derivatives (figure 6*b*, *c*), remain unchanged if compared to figure 5(*b*, *c*). As we expected, the correlation curves calculated from equation (2.4), the second estimator $\overline{\rho_{XY}}$, for the longer-scale processes are significantly different from the respective ones calculated with the first estimator ρ_{XY}. This is due to the 'over-estimation' bias of ρ_{XY} caused by strong events as discussed above.

We are aware that by assigning to the contribution of each trajectory the same weight in the second estimator, i.e. averaging all the single correlation coefficients, we obtain the averaged correlation curves $\overline{\rho_{XY}}$ that represent the 'most common' (not necessarily the 'true') behaviour. The difference between the most common and the true behaviour is related to the effect of the co-occurrence of high-strain and high-enstrophy for a relatively long portion of the trajectory, which was for example reported by Zeff *et al.* (2003). In order to single out this effect we compute the cross-correlation ρ_{XY} (equation (2.2)) between strain and enstrophy excluding a certain percentage of trajectories characterized by high-strain and high-enstrophy. In particular we set a condition on the contribution to the variance of each single trajectory ($Var(s^2)_{ti}$ or $Var(\omega^2)_{ti}$). Dataset A includes all the trajectories and two other datasets have been created for comparison. In dataset B we exclude the top 5 % of the trajectories sorted according to their variance. Dataset C, which excludes 15 % of those displaying highest strain or enstrophy variance, is the moderate set. In figure 8 we show the cross-correlation between ω^2 and s^2 and between $\omega_i\omega_j s_{ij}$ and $-s_{ij}s_{jk}s_{ki}$ for the three different datasets.

We observe that the peak of the correlation curves becomes lower when going from set A to B and C, especially for ω^2 and s^2. Apparently, this effect is due to the contribution to the positive ω^2 and s^2 cross-correlation, given by some strong and rare events. We infer that the influence of strong events is observed less for the correlation between the production terms since their time scales are shorter: in fact a trajectory $10\tau_\eta$ long is likely to be influenced by strong production events only for a short time.

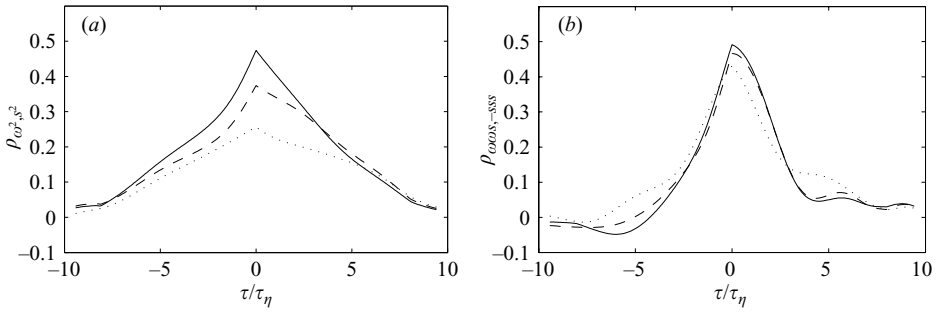

FIGURE 8. Lagrangian cross-correlation functions between (a) strain and enstrophy, and (b) their production terms $\omega_i\omega_j s_{ij}$ and $-s_{ij}s_{jk}s_{ki}$, computed using equation (2.2), estimator ρ_{XY} on three different datasets: A (continuous line) whole set of trajectories, B (— — —) 3 % high-strain (or high-enstrophy) trajectories excluded, C (···) 14 % high-strain (or high enstrophy) trajectories excluded.

We expect the third estimator $\widehat{\rho_{XY}}$ (equation (2.6)) to overcome, at least in part, some of the bias present in the first two estimators, because it is taking into account the effect of rare and strong events by weighting the contribution of each trajectory to R_{XY} with its own variance. The results shown in figure 7 support this expectation: the peak of the cross-correlation function between ω^2 and s^2 is lower in figure 7(a) than figure 5(a), while the other curves (with shorter time scales) depict the same behaviour as shown in figure 5. In order to strengthen our interpretation of the effect of the estimators, we carry out a comparative analysis between the second and the third estimators on the full and the 'tame' datasets (A and C respectively). The results are shown in figure 9. As anticipated, $\overline{\rho_{XY}}$ is not affected by the strong events as shown by comparing figures 9(b) and 9(d). It is striking that for the tame dataset, $\overline{\rho_{XY}}$ and $\widehat{\rho_{XY}}$ show exactly the same shape. In addition, the comparison between figures 9(a) and 9(c) implies that the only contribution to the positive cross-correlation between strain and enstrophy at $\tau = 0$ is from rare and strong events and it is thus due to the overestimation bias.

From the analysis of the three different estimators we conclude that, in case of trajectories of finite length, all three are necessary for a meaningful interpretation of the correlation results. Enstrophy and strain at zero time lag behave quite independently (in the sense that they show vanishing correlation in the 'most common' case), in other words most of the time they are not 'in phase'. Nevertheless, they are positively correlated (shown by estimators 1 and 3) due the contribution by rare events in which both quantities are high (still with no implication of being in phase or not), due to the overestimation bias. Because of the events in which both s^2 and ω^2 are high, one can assume that there is a probability that they grow simultaneously, but then we would observe a positive correlation at $\tau = 0$ between $\mathrm{D}\omega^2/\mathrm{D}t$ and $\mathrm{D}s^2/\mathrm{D}t$, which does not seem to be the case (regardless of the estimator). As is also expected, $\omega_i\omega_j s_{ij}$ and $-s_{ij}s_{jk}s_{ki}$ maintain a degree of correlation in time, regardless of the type of estimator we use. The fact that enstrophy and strain are not in phase, $\mathrm{D}\omega^2/\mathrm{D}t$ and $\mathrm{D}s^2/\mathrm{D}t$ are not correlated at zero time lag, but the processes of strain and enstrophy production often occur at the same location, and at the same time, is another strong indication that non-local processes play an important role in strain and enstrophy dynamics. In order to address some further questions, such as the effect of positive $\omega_i\omega_j s_{ij}$ on the evolution of strain, in the next section we investigate the cross-correlation functions under the four conditions.

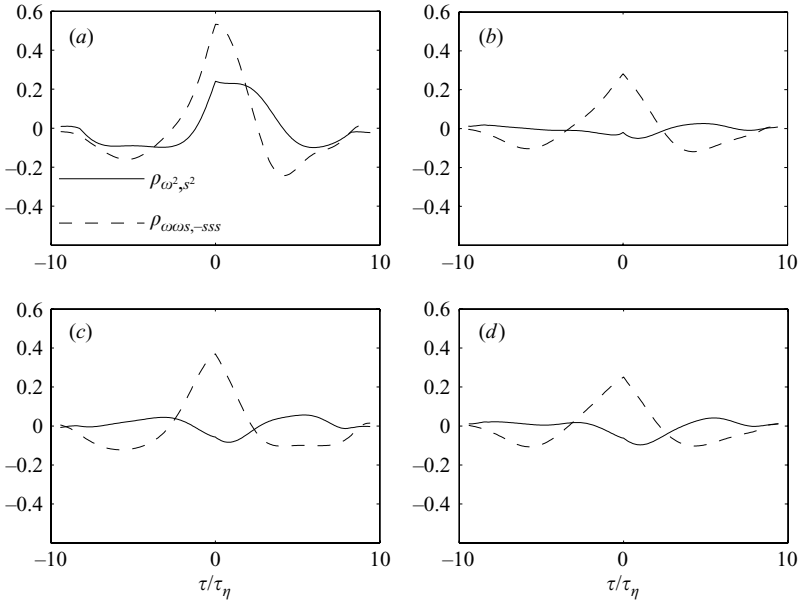

FIGURE 9. Lagrangian cross-correlation functions between strain and enstrophy (and their production terms), computed using: (*a*) estimator $\widehat{\rho}_{XY}$ on dataset A, (*b*) estimator $\overline{\rho_{XY}}$ on dataset A, (*c*) estimator $\widehat{\rho}_{XY}$ on dataset C, (*d*) estimator $\overline{\rho_{XY}}$ on dataset C. Note that non-weighted contributions are not affected by the presence of strong events (*b*, *d*), while weighted contributions (*a*, *c*) show weaker correlation for the 'tamer' set of trajectories. In the latter case, consistently, the two procedure give the same results (*c*, *d*).

3.4. *Conditioned cross-correlation functions*

Similarly to the analysis in § 3.2 we use the following conditions: i) high-strain–low-enstrophy ii) high strain–high-enstrophy, iii) low-strain–high-enstrophy, iv) low-strain–low-enstrophy. As for conditioned autocorrelation functions, two sets of cross-correlation functions are shown, following the different criteria that define the 'high' and 'low' conditions. In particular, figures 10, 11 and 12 were estimated with a threshold value chosen such as to include only the bottom or top 30 % of the strain and enstrophy distributions respectively. In the curves shown in figures 13–15, 'high' and 'low' conditions are defined as larger and smaller than the mean value.

In figures 10 and 11 we show the cross-correlation functions between the terms under investigation. In each figure four different line types depict the four different conditions. The results of the estimators 1, 2 and 3 are given from left to right, respectively. It is noteworthy that, regardless of the estimator employed, the shapes of the conditioned correlation functions in figures 10 and 11 exhibit the same qualitative behaviour. It is also observed for the other cross-correlation functions, which are shown in figure 12 for the first estimator only. We observe that strain and its production term are well-correlated ($\rho_{s^2,-sss}(\tau=0)\approx 0.5$) especially when strain is high (solid line and line with dots). It is interesting that they are also well-correlated when both strain and enstrophy are weak, and only under high-enstrophy–low-strain condition does this correlation vanishes. This might be related to the shorter autocorrelation time scale exhibited by $-s_{ij}s_{jk}s_{ki}$ under the same conditions (see figure 3) and possibly due to the effect of the increased rotation of the strain eigenframe in vorticity-dominated regions.

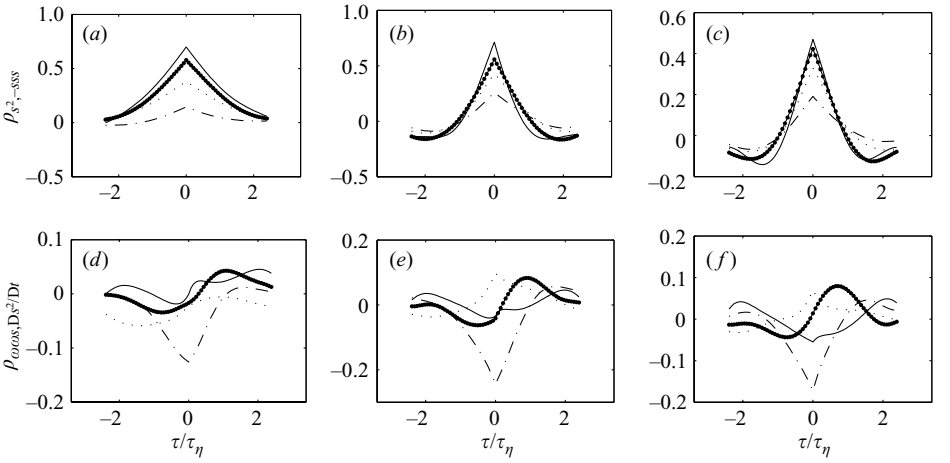

FIGURE 10. Lagrangian cross-correlation functions $\rho_{s^2,-sss}$ and $\rho_{\omega\omega s,\mathrm{D}s^2/\mathrm{D}t}$ for conditioned trajectory samples: high-strain–low-enstrophy (—), high-strain–high-enstrophy (-●-●-●-), high-enstrophy–low-strain (·—·—·), low-enstrophy–low-strain (· · ·). Correlations are computed following the three procedures: (a, d) $\rho_{XY}(\tau)$, (b, e) $\overline{\rho}_{XY}(\tau)$, (c, f) $\widehat{\rho}_{XY}(\tau)$.

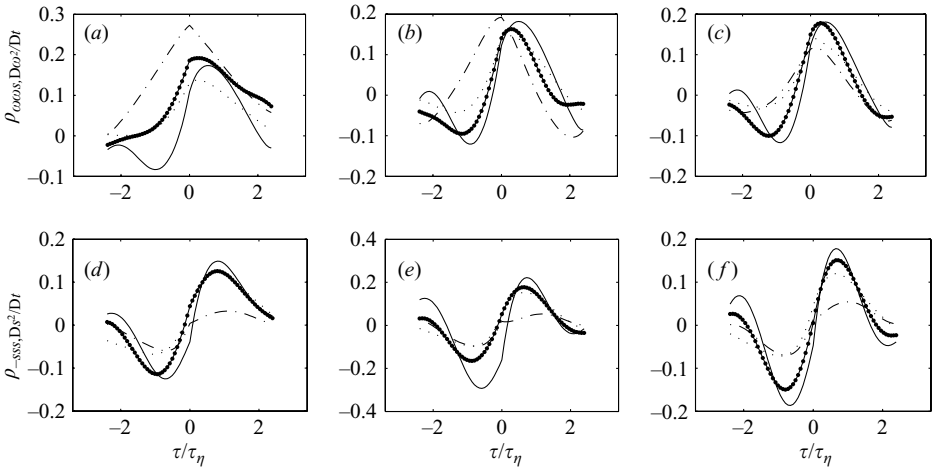

FIGURE 11. Lagrangian cross-correlation functions $\rho_{\omega\omega s,\mathrm{D}\omega^2/\mathrm{D}t}$ and $\rho_{-sss,\mathrm{D}s^2/\mathrm{D}t}$ for conditioned trajectory samples: high-strain–low-enstrophy (—), high-strain–high-enstrophy (-●-●-●-), high-enstrophy–low-strain (·—·—·), low-enstrophy–low-strain (· · ·). Correlations are computed following the three procedures: (a, d) $\rho_{XY}(\tau)$, (b, e) $\overline{\rho}_{XY}(\tau)$, (c, f) $\widehat{\rho}_{XY}(\tau)$.

In high-enstrophy–low-strain regions we discover that the enstrophy production term is locally correlated with the material derivative of enstrophy (figure 11*a–c*), but also significantly negatively correlated with the strain derivative meaning that, in high-enstrophy regions, positive vortex stretching is associated with the decrease of s^2 (figure 10*d–f*).

In our interpretation, the high-enstrophy–low-strain regions are essentially different from the rest of the flow regions. We notice that under all other conditions, the peak of the correlation functions between $\omega_i\omega_j s_{ij}$ and the material derivatives is shifted towards non-zero time lags (different types of the correlation function suggest different types of interaction). The non-zero time lag is an important difference between the

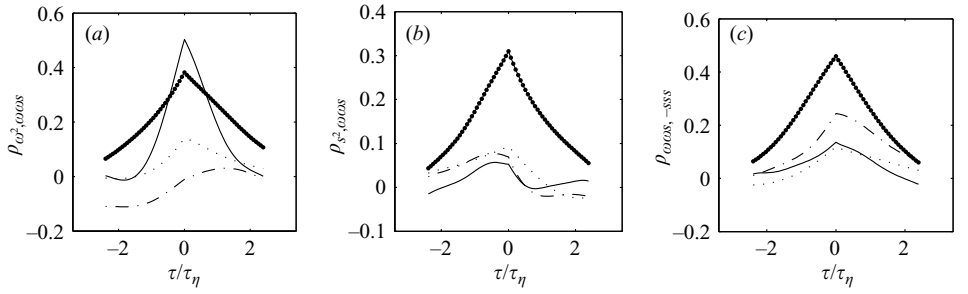

FIGURE 12. Lagrangian cross-correlation functions $\rho_{\omega^2,\omega\omega s}$, $\rho_{s^2,\omega\omega s}$, and $\rho_{\omega\omega s,sss}$ for conditioned trajectory samples: high-strain–low-enstrophy (—), high-strain–high-enstrophy (-●-●-●-), high-enstrophy–low-strain (·—·—·), low-enstrophy–low-strain (· · ·). Correlations are computed using the estimator $\rho_{XY}(\tau)$.

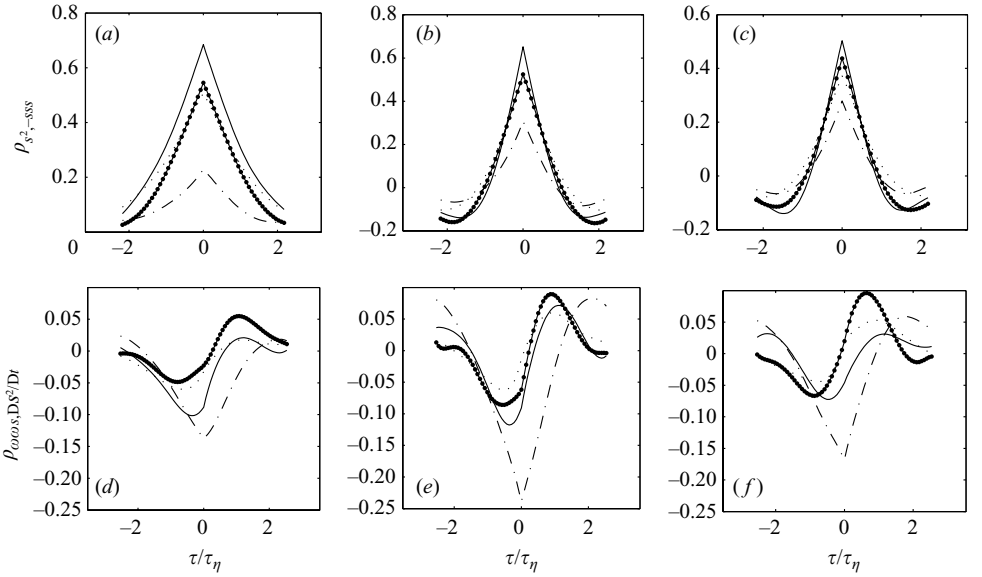

FIGURE 13. Lagrangian cross-correlation functions $\rho_{s^2,-sss}$ and $\rho_{\omega\omega s,\mathrm{D}s^2/\mathrm{D}t}$ for conditioned trajectory samples (larger, smaller than the mean): high-strain–low-enstrophy (—), high-strain–high-enstrophy (-●-●-●-), high-enstrophy–low-strain (·—·—·), low-enstrophy–low-strain (· · ·). Correlations are computed following the three procedures: (a, d) $\rho_{XY}(\tau)$, (b, e) $\overline{\rho}_{XY}(\tau)$, (c, f) $\widehat{\rho}_{XY}(\tau)$.

cross-correlation functions of $\rho_{\omega\omega s,\mathrm{D}\omega^2/\mathrm{D}t}$ and $\rho_{-sss,\mathrm{D}s^2/\mathrm{D}t}$ (compare figure 11$(a–c)$ and figure 11$(d–f)$). On the one hand, it is a commonplace that in strain-dominated regions the derivative of enstrophy (which is not directly connected to the strain in its equation (1.2)) is correlated with the enstrophy production after a certain delay in time. On the other hand it is interesting to note that $-s_{ij}s_{jk}s_{ki}$ and $\mathrm{D}s^2/\mathrm{D}t$ are more correlated at $\tau \neq 0$, and under all conditions. This is another clear indication that non-local effects are intimately associated with strain growth.

In figure 12(a) $\rho_{\omega^2,\omega\omega s}$ in high-strain–low-enstrophy regions (solid line) displays a significant correlation of about 0.5 at $\tau = 0$ and it is less skewed compared to the curves for the other conditions (similar to the results in figure 13(a). The lack of skewness suggests that vortex stretching in high-strain–low-enstrophy regions is not as efficient,

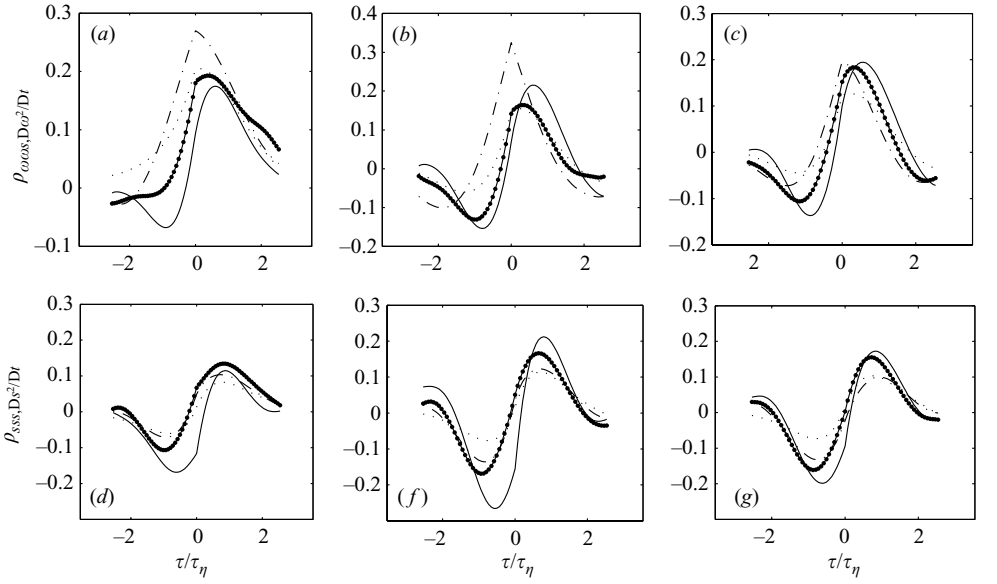

FIGURE 14. Lagrangian cross-correlation functions $\rho_{\omega\omega s,\mathrm{D}\omega^2/\mathrm{D}t}$ and $\rho_{-sss,\mathrm{D}s^2/\mathrm{D}t}$ for conditioned trajectory samples (larger, smaller than the mean): high-strain–low-enstrophy (—), high strain–high-enstrophy (-•-•-•-), high enstrophy–low-strain (·—·—·), low-enstrophy–low strain (···). Correlations are computed following the three procedures: (a, d) $\rho_{XY}(\tau)$, (b, e) $\overline{\rho}_{XY}(\tau)$, (c, f) $\widehat{\rho}_{XY}(\tau)$.

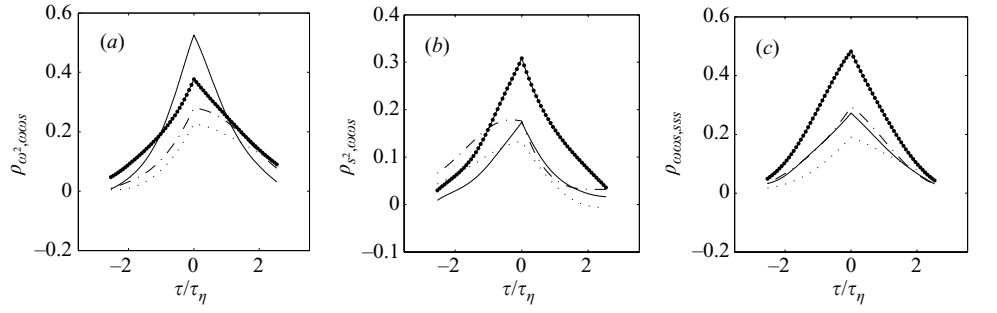

FIGURE 15. Lagrangian cross-correlation functions $\rho_{\omega^2,\omega\omega s}$, $\rho_{s^2,\omega\omega s}$, and $\rho_{\omega\omega s,sss}$ for conditioned trajectory samples (larger, smaller than the mean): high-strain–low-enstrophy (—), high-strain–high-enstrophy (-•-•-•-), high-enstrophy–low-strain (·—·—·), low-enstrophy–low-strain (···). Correlations are computed using the estimator $\rho_{XY}(\tau)$.

statistically, as in the case of high-strain–high-enstrophy. Therefore we can infer that the high-strain–low-enstrophy flow regions are the result of the self-amplification of strain (i.e. $-s_{ij}s_{jk}s_{ki}$) with no or little effect on enstrophy production. This is supported by the two other trends: (i) in low-strain–low-enstrophy $\rho_{s^2,-sss}(\tau = 0)$ is as significant as in high-strain conditions (figure 10*a–c*), implying that $\rho_{s^2,-sss}$ shows significant correlation as long as enstrophy is low; (ii) in high-strain–low-enstrophy regions the correlation between $\omega_i\omega_j s_{ij}$ and $-s_{ij}s_{jk}s_{ki}$ is weak (figure 12*c*), implying that enstrophy production in high-strain–low-enstrophy regions is not correlated with strain production. We also observe that, when strain is low, $\rho_{s^2,\omega\omega s}$ and $\rho_{\omega^2,\omega\omega s}$ are

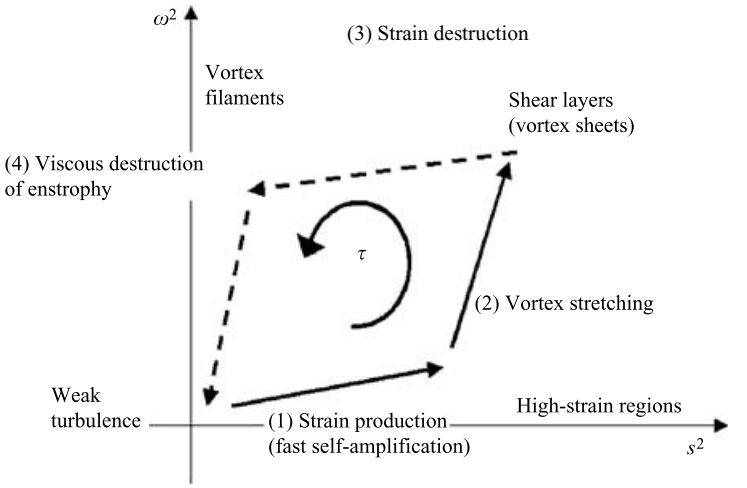

FIGURE 16. Qualitative description of the processes contributing to maintain strain and enstrophy in equilibrium.

skewed in the opposite direction (figure 13*a*), indicating that $\omega\omega s$ is statistically followed by larger ω^2 and anticipated by larger s^2.

A possible interpretation of the results in this sections is that strain production statistically anticipates enstrophy production (as it was inferred from unconditioned cross-correlation functions in figure 7*d*). The fact that $\rho_{s^2,\omega\omega s}$ is relatively low is not surprising, if we recall that the interaction between enstrophy and strain is strongly dependent on the alignment between ω and the eigenvectors of the rate of strain tensor λ_i (Lüthi *et al.* 2005 and Guala *et al.* 2005). Hence, on the one hand, we infer that high magnitude of the rate of strain does not necessarily induce high enstrophy production. On the other hand enstrophy production exhibits higher values if conditioned on strain magnitude rather than on enstrophy magnitude (Tsinober 2001). It is important to note that the two statements are not in contradiction. In fact, the rare events of high-strain and ω aligned with the eigenvector λ_1 (associated with the largest positive eigenvalue), contribute more significantly to positive $\omega_i\omega_j s_{ij}$, compared to the statistically predominant situation of high-strain regions in which ω is aligned with the eigenvector λ_2 (associated with the intermediate eigenvalue).

3.5. *Discussion*

In this section we discuss our results and suggest a physical interpretation of the investigated auto- and cross-correlation functions. We attempt to present a qualitative picture in which we connect the different regions associated with the imposed conditions with the various processes of strain and enstrophy dynamics. Schematically, the picture is given in figure 16. The solid lines emphasize the direction of growth of the quantity on the axis and the dashed lines emphasize their destruction. Only four major 'vectors' are shown, each referring to one of the statistically detected processes as we discuss below. We cannot claim that there are no other processes, connecting the different situations shown in figure 16, but they are not detected by the correlation analysis. For example, we are unable to conclude anything about processes like vortex reconnection or vortex breakdown, since their occurrence is not reflected in our results.

We have indications that in low-strain–low-enstrophy regions, strain is the first to increase through the known strain self-amplification process (Tsinober 2001): in figures 5(*d*) and 7(*d*) we observe positive $\mathrm{D}\omega^2/\mathrm{D}t$ 'anticipating' positive $\mathrm{D}s^2/\mathrm{D}t$. In figure 10 in low-enstrophy–low-strain conditions s^2 and $-s_{ij}s_{jk}s_{ki}$ are positively correlated similarly to the high-strain regions and definitely more correlated than in high-enstrophy–low-strain regions. In addition in figure 12(*c*) in low-strain–low-enstrophy regions the correlation curve is significantly skewed to positive time lags, meaning that positive $\omega_i\omega_j s_{ij}$ 'follows' positive $-s_{ij}s_{jk}s_{ki}$. Enstrophy production is the major process responsible for the evolution of high-strain–low-enstrophy regions into high-strain–high-enstrophy regions. The differences are emphasized in figure 12 and figure 11(*a–c*). This is in agreement with the findings by Andreotti *et al.* (2001) regarding the production of vorticity by shear instability in high-strain regions. We find that the regions of high-strain–high-enstrophy (possibly related to shear layers or vortex sheets) are the most important ones for the strain and vorticity production processes. We observe that in these regions the production of strain and the production of enstrophy are simultaneous processes (figure 12*c*) which are followed by a significant growth of strain and enstrophy (figure 11). However we have some indication that strain production becomes less efficient as in low-enstrophy regions. In figures 10(*a–c*) and 11(*d–f*), the peaks of the correlation coefficients $\rho_{s^2,-sss}$ and $\rho_{-sss,\mathrm{D}s^2/\mathrm{D}t}$ in the case of high-strain–high-enstrophy, are lower than in the case of high-strain–low-enstrophy. The less efficient strain production combined with strong and positive $\omega_i\omega_j s_{ij}$ would eventually lead to the reduction of $\mathrm{D}s^2/\mathrm{D}t$ as follows from equation (1.1). Even without including the effect of other important processes (see § 1), this may explain why regions of high-strain–high-enstrophy statistically evolve into regions of high-enstrophy–low-strain. This deduction is also in full agreement with the results of Cao *et al.* (1999) and Brachet *et al.* (1992) among others, who observed the formation of vortex filaments (worms) from vortex sheets (shear layers), and with the fact that vortex filaments are known to be associated with relatively long time scales compared to the time scale typical of high-strain regions (see for example Jimenez & Wray (1998) and Vincent & Meneguzzi (1994) among others).

The regions of high enstrophy and low strain are very different from the others, in the sense that: (i) positive enstrophy production is correlated with the depletion of strain (figure 10, bottom), and with the increase of enstrophy (figure 11 top); (ii) the correlations between strain and its production (figure 10top) and between strain production and strain derivative (figure 11 bottom) vanish. In such regions, since strain and its production are low and ω is known to be predominantly aligned with λ_2 (Tsinober 2001), we may infer that $\omega_i\omega_j s_{ij}$ cannot balance the viscous destruction of enstrophy (equation (1.2)). Thus high-enstrophy–low-strain regions will most probably evolve into low-enstrophy–low-strain regions due to the effect of the viscous terms.

4. Conclusions

Lagrangian autocorrelation functions of the rate of strain, s^2, enstrophy, ω^2, their production terms $-s_{ij}s_{jk}s_{ki}$, $\omega_i\omega_j s_{ij}$ and material derivatives, $\mathrm{D}s^2/\mathrm{D}t$ and $\mathrm{D}\omega^2/\mathrm{D}t$, respectively, were calculated by using the experimental results of Lüthi *et al.* (2005) in homogeneous turbulent flow with $Re_\lambda = 50$. The main point of this contribution is to provide a set of Lagrangian auto- and cross-correlation functions between strain, enstrophy and the related terms from experimental data, with the main goal of clarifying some aspects of the dynamics of s^2 and ω^2. Some issues related to the use of different estimators in the computation of correlation functions have been

thoroughly investigated. In particular, we have analysed the bias effects due to the finite length of the trajectories, the normalization with different variance estimators, and the time scales of the investigated processes.

The comparative behaviour of the strain and enstrophy autocorrelations is in reasonable agreement with the results obtained from numerical simulations (Yeung & Pope 1989; Yeung 2001; Mordant *et al.* 2004). Owing to the combined effect of the biased estimator and the limited size of the samples (the trajectory time length is not much larger than the time scale of the flow), the velocity and enstrophy integral scales are underestimated in our process. Nevertheless, the integral time scales of shorter-scale processes (such as strain and the production terms) agree well with the previous results.

Through the conditioned autocorrelation functions we observe that the scales of the investigated processes are quantitatively different depending on the magnitude of strain and enstrophy. In particular it is shown that in high-strain–low-enstrophy regions $\omega_i\omega_j s_{ij}$ becomes a shorter-scale process while in high-enstrophy–low-strain regions it is $-s_{ij}s_{jk}s_{ki}$ which displays a shorter time scale. In a similar manner, cross-correlation functions between the various terms have been computed with and without the conditions on the levels of strain and enstrophy.

Despite the underestimation of the skewness of the cross-correlation curve between ω^2 and s^2, the level of the peak at zero time lag is obtained in agreement with the results of Yeung & Pope (1989) and Mordant *et al.* (2004). The main result is that ω^2 and s^2 do not grow and decay simultaneously, which is another indication that non-local processes play a crucial role in small-scale dynamics. In particular it is inferred that the statistical evolution of strain and enstrophy can be summarized in a sequence of processes (e.g. figure 16) starting with the strain self-amplification in low-strain–low-enstrophy regions, followed by enstrophy production and growth, leading to the formation of high-strain–high-enstrophy regions. The depletion of both strain and its production in parallel with the growth of enstrophy is related to the evolution of these regions into high-enstrophy–low-strain regions or, in other words, to the evolution of vortex sheets (shear layers) into vortex filaments. It is speculated that these regions evolve into low-enstrophy–low-strain regions since the enstrophy production, in the presence of low strain and preferential alignment between ω and λ_2, cannot balance the viscous destruction of enstrophy.

We must stress that the sequential picture of these processes, sketched in figure 16, is distinctly qualitative, though inferred from statistical results, and should not be taken literally. For example, one arrow in figure 16 does not mean that we can describe the evolution of high-enstrophy–low-strain regions into a weak turbulence situation as a one-step process. The sketch shows only the general trends and relations that could be detected statistically by means of the correlation analysis. Nevertheless, if we address the question of how in a stationary homogeneous turbulent flow $\langle s^2\rangle$ and $\langle\omega^2\rangle$ become statistically steady, this statistical analysis suggests the qualitative picture of a cyclic sequence of local and non-local processes of different Lagrangian time scales. It is quite clear that several essential aspects of these processes require more detailed study including the use of more sophisticated tools than those used here. We acknowledge two major limitations in the present work: (i) the experiments were performed in a low Reynolds number flow; (ii) the subsets of trajectories defined as high-strain (enstrophy) are conditioned on a threshold value which is not large enough to allow a discussion of intermittency effects. The second limitation is even more restrictive for high Reynolds number flows, implying that the extension of the presented results to such flows is questionable. One particular aspect is the difference

between the time scales of strain and enstrophy. Numerical results from Yeung & Pope (1989) and Yeung (2001) seemingly show that the ratio T_{s^2}/T_{ω^2} tends to unity with increase of the Reynolds number. In this context the sequential picture of different time-scale processes previously discussed might be revised for high Reynolds number flows. It is however noteworthy that, in terms of Eulerian statistics, there is a qualitative resemblance between the statistical property of $\omega_i\omega_j s_{ij}$, $s_{ij}s_{jk}s_{ki}$, the alignment between ω and the eigenvectors of the rate of strain tensor λ_i, and other small-scale properties shown in Lüthi *et al.* (2005) and Guala *et al.* (2005), with the corresponding statistics obtained at $Re_\lambda = 10^4$ by Kholmyansky, Tsinober & Yorish (2001). Also, in the present analysis we could not assess the pressure–strain interaction and the viscous terms $-s_{ij}\partial^2 p/(\partial x_i \partial x_j)$, $\nu s_{ij}\nabla^2 s_{ij}$ and $\nu\omega_i\nabla^2\omega_i$, which definitely deserve further investigation, even at such low Reynolds number.

REFERENCES

Andreotti, B., Douady, S. & Couder, Y. 2001 An experiment on two aspects of the interaction between strain and vorticity. *J. Fluid Mech.* **444**, 151–174.

Brachet, M. E., Meneguzzi, M., Vincent, A., Politano, H. & Sulem, P. L. 1992 Numerical evidence of smooth self-similar dynamics and possibility of subsequent collapse for three-dimensional ideal flows. *Phys. Fluids* A **4**, 2845–2854.

Cao, N., Chen, S. & Doolen, G. D. 1999 Statistics and structures of pressure in isotropic turbulence. *Phys. Fluids* **11**, 2235–2250.

Chacin, J. & Cantwell, B. J. 2000 Dynamics of a low Reynolds number turbulent boundary layer. *J. Fluid Mech.* **404**, 87–115.

Chong, M. S. & Perry, A. E. 1990 A general classification of three dimensional flow fields. *Phys. Fluids* A **2**, 765–777.

Constantin, P. 1994 Geometric statistics in turbulence. *SIAM Rev.* **36**, 73–98.

Guala, M., Lüthi, B., Liberzon, A., Kinzelbach, W. & Tsinober, A. 2005 On the evolution material lines and vorticity in homogeneous turbulence. *J. Fluid Mech.* **533**, 339–359.

Jeong, E. & Girimaji, X. 2003 Velocity gradient dynamics in turbulence: effect of viscosity and forcing. *J. Theor. Comput. Fluid Dyn.* **16**, 421–432.

Jimenez, J. & Wray, A. A. 1998 On the characteristic of vortex filaments in isotropic turbulence. *J. Fluid Mech.* **373**, 255–285.

Kholmyansky, M., Tsinober, A. & Yorish, S. 2001 Velocity derivatives in the atmospheric surface layer at $Re_\lambda = 10^4$. *Phys. Fluids* **13**, 311–314.

Lüthi, B. 2002 Some aspects of strain, vorticity and material element dynamics as measured with three-dimensional particle tracking velocimetry in a turbulent flow. PhD Dissertation, Swiss Federal Institute of Technology, ETHZ.

Lüthi, B., Tsinober, A. & Kinzelbach, W. 2005 Lagrangian measurement of vorticity dynamics in turbulent flow. *J. Fluid Mech.* **528**, 87–118.

Martin, J. N., Ooi, A., Chong, M. S. & Soria, J. 1998 Dynamics of the velocity gradient tensor invariants in isotropic turbulence. *Phys. Fluids* **10**, 2336–2346.

Monin, A. S. & Yaglom, A. M. 1971 *Statistical Fluid Mechanics, The Mechanics of Turbulence*, New English edition vol. 1, Chapters 2 and 3. CTR Monographs, NASA Ames – Stanford University.

Monin, A. S. & Yaglom, A. M. 1975 *Statistical Fluid Mechanics, The Mechanics of Turbulence*, vol. 2. CTR Monographs, NASA Ames – Stanford University.

Mordant, N., Leveque, E. & Pinton, J. F. 2004 Experimental and numerical study on the Lagrangian dynamics of high Reynolds turbulence. *New J. Phys.* **6**, 116.

Nomura, K. K. & Post G. K. 1998 The structure and dynamics of vorticity and rate of strain in incompressible homogeneous turbulence. *J. Fluid Mech.* **377**, 65–97.

Ooi, A., Martin, J. N., Chong, M. S. & Soria, J. 1999 A study of the evolution and characteristics of the invariants of the velocity gradient tensor in isotropic turbulence. *J. Fluid Mech.* **381**, 141–174.

Pope, S. B. 1990 Lagrangian microscales in turbulence. *Phil. Trans. R. Soc. Lond.* **333**, 309–319.

Priestley, M. B. 1981 *Spectral Analysis and Time Series*. Academic.

Taylor, G. I. 1921 Diffusion by continuous movements. *Proc. R. Soc. Lond.* A **100**, 114–121.

Tennekes, H. & Lumley, J. L. 1972 *A First Course in turbulence*. MIT Press.

Tsinober, A. 2000 Vortex stretching versus production of strain/dissipation. In *Turbulence Structure and Vortex Dynamics* (ed. J. C. R. Hunt & J. C. Vassilicos), pp. 164–191. Cambridge University Press.

Tsinober, A. 2001 *An Informal Introduction to Turbulence*. Kluwer.

Vincent, A. & Meneguzzi, M. 1994 The dynamics of vorticity tubes in homogeneous turbulence. *J. Fluid Mech.* **258**, 245–254.

Yeung, P. K. 2001 Lagrangian characteristics of turbulence and scalar transport in direct numerical simulation. *J. Fluid Mech.* **427**, 24–274.

Yeung, P. K. 2002 Lagrangian investigation of turbulence. *Annu. Rev. Fluid Mech.* **34**, 115–142.

Yeung, P. K. & Pope, S. B. 1989 Lagrangian statistics from direct numerical simulation of isotropic turbulence. *J. Fluid Mech.* **207**, 531–586.

Zeff, B. W., Lanterman, D. D., McAllister, R., Rajarshi, R., Kostelich, E. J. & Lathrop, P. 2004 Measuring intense rotation and dissipation in turbulent flows. *Nature* **421** 146–149.